



AGN and starbursts in the HDF-N and HFF : Deep, global VLBI observations

S. Chi^{1,2,3}, M. A. Garrett^{2,4,5}, and P. D. Barthel¹

¹ Kapteyn Astronomical Institute, Rijksuniversiteit Groningen, P. O. Box 800, 9700 AV Groningen, The Netherlands, e-mail: chi@astro.rug.nl

² ASTRON, P. O. Box 2, 7990 AA Dwingeloo, The Netherlands

³ JIVE, P. O. Box 2, 7990 AA Dwingeloo, The Netherlands

⁴ Centre for Astrophysics and Supercomputing, Swinburne University of Technology, Mail number H39, P. O. Box 218, Hawthorn, Victoria 3122, Australia

⁵ Leiden Observatory, P. O. Box 9513, 2300 RA Leiden, The Netherlands

Abstract. We present the results of deep, wide-field global VLBI 1.4 GHz observations of the Hubble Deep Field North (HDF-N) region and the surrounding Hubble Flanking Fields (HFF). Using the global VLBI network, we attained an r.m.s. noise level of $7 \mu\text{Jy}/\text{beam}$ with a 4 mas angular resolution in the inner part of the field. Above the 5σ detection level, we clearly detected 12 compact radio sources. The observations strongly suggest that these sources harbour AGN. Some of the sources show resolved structures, in particular we resolved a jet-like extension emanating from the AGN core of a distant, dust-obscured starburst galaxy. We calculated the ratio between $S_{24\mu\text{m}}$ and $S_{1.4\text{ GHz}, Q_{24\mu\text{m}}}$, for our sample, and discuss correlations between the mid-IR, X-ray, and radio luminosities. The results clearly demonstrate the power of deep, high-resolution VLBI imaging in discriminating between star-formation and AGN activity in distant, dust-obscured systems.

Key words. galaxies: active – galaxies: radio continuum – galaxies: starburst

1. Introduction

High sensitivity radio observations of the Hubble Deep Field North (HDF-N) and its surrounding Flanking Field (HFF) have revealed a population of faint sub-mJy and μJy radio sources, which appear to be associated with high-redshift, star-forming galaxies (Richards et al. 1998, 1999; Richards 2000; Garrett et al. 2001; Muxlow et al. 2005). One of the most remarkable results of the radio-optical study of these fields was the discovery

of a number of optically-faint radio sources, some of which are undetected in the deepest optical images. These optically faint systems are thought to be distant, dust-obscured galaxies. Recent *Spitzer* imaging of a sub-mm galaxy sample suggested that their IR luminosities are dominated by star-formation rather than nuclear activities (Pope et al. 2006). On the other hand, some of the sources present both properties of a starburst galaxy and an AGN, which lead the interpretation to a hybrid system (dusty starburst+embedded AGN). Such systems are only detectable in the radio and/or sub-mm, and deep, high angular reso-

Send offprint requests to: S. Chi

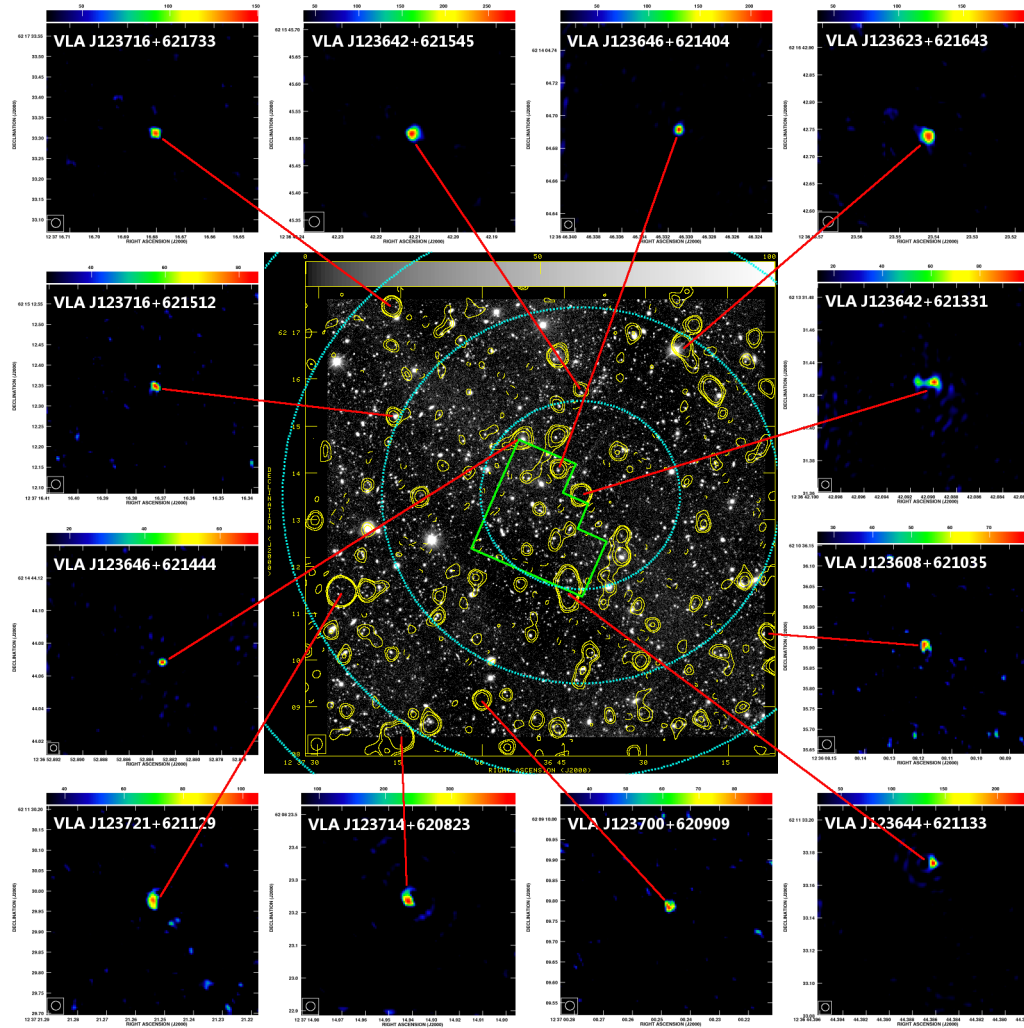


Fig. 1. The center image is a WSRT 1.4 GHz contour map superposed on CFHT *I*-band image (Garrett et al. 2000). The HDF-N region is represented by solid green line and the four annular fields (2', 4', 6', and 8' radius from the correlation phase center) are indicated with dotted blue circles. Each of the fields has different sensitivity ($7\sim 37 \mu\text{Jy}/\text{beam}$) and angular resolution ($4\sim 27 \text{ mas}$) due to image tapering. Surrounding it are the 12 images of the radio sources detected in the HDF-N and HFF, whose color scales range from 3σ to the peak intensity level of each source.

lution radio observations are currently the best way to discriminate those embedded AGN.

In this workshop, we present the results of deep, wide-field global VLBI 1.4 GHz observations of the HDF-N and HFF. In addition, we also discuss possible correlations between the mid-IR, X-ray, and radio luminosities.

2. Global VLBI observations

Observations of the HDF-N and HFF region were made with a global VLBI array on 20–22 February 2004 at 1.4 GHz. A total 36 hours observing time was split into three, 12-hours runs. The global VLBI array consisted of 16 telescopes in Europe and the USA, and

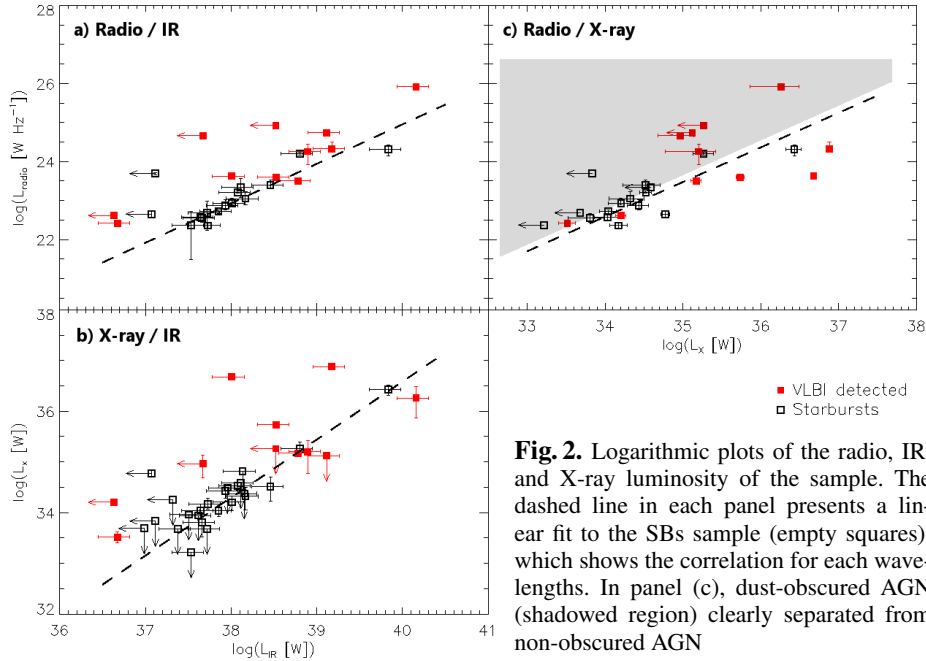


Fig. 2. Logarithmic plots of the radio, IR, and X-ray luminosity of the sample. The dashed line in each panel presents a linear fit to the SBs sample (empty squares), which shows the correlation for each wavelengths. In panel (c), dust-obscured AGN (shadowed region) clearly separated from non-obscured AGN

data recorded at a bit rate of 128 Mbits/s in both right (R)- and left (L)-hand circular polarisation. The observations were made in phase-referencing mode with ~ 19 hours of total on-source integration time on the HDF-N. Two phase-calibrators were used, the strong primary calibrator J1241+602 ($S_{1.4 \text{ GHz}} \sim 455$ mJy) and the fainter secondary calibrator J1234+619 ($S_{1.4 \text{ GHz}} \sim 20$ mJy). More frequent scans on this nearby, secondary calibrator allowed us to obtain the finer phase corrections.

The data were processed at the European VLBI Network (EVN) correlator at JIVE, in Dwingeloo, the Netherlands. Each 8 MHz band (R&L) was correlated in separate passes in order to maximise spectral resolution (256 channels/IF) and so to minimise bandwidth smearing. An integration time of 0.25 seconds was employed to reduce the effects of time smearing. The data from each IF were averaged, edited, and calibrated with the NRAO AIPS package, and then the gain parameters applied to the unaveraged original data.

In order to image out the entire HDF-N and HFF, the wide-field imaging technique was used (Garrett et al. 1999). We generated 92 dirty images and dirty beams from each 8 MHz band (R&L simultaneously) using IMAGR and co-added respectively – field with a clear detection were then CLEANed using APCLN.

3. Observational results

The wide-field global VLBI survey covered a total of 201 square-arcmin divided into four annular fields with different sensitivities and angular resolutions (Fig. 1). The observations are both deeper and wider than any previous VLBI observations of the field, attaining an r.m.s. noise level of $7.3 \mu\text{Jy}/\text{beam}$ with 4 mas angular resolution in the HDF-N. For the outer fields, each annulus has different sensitivity ($14 \sim 37 \mu\text{Jy}/\text{beam}$) and angular resolution ($19 \sim 27$ mas). In these fields, we imaged out all of 92 radio sources, which were detected by the MERLIN-VLA survey (Muxlow et al. 2005). Given the different sensitivities in each annulus

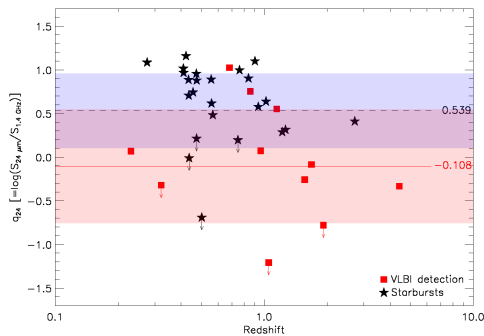


Fig. 3. The $q_{24\mu\text{m}}$ for SBs (star) and 12 global VLBI detections (squares). Dashed and solid lines represent the mean value for each sample, respectively, and, the 1σ deviation is shown by a colored region.

and the VLA flux densities of the sources, 48 radio sources out of 92 targets should be bright enough to be detected by our observations.

The new global VLBI observations clearly revealed 12 (out of 48) radio sources in the HDF-N and HFF above the 5σ detection level, which correspond to $\sim 25\%$ of detection rate. The global VLBI detections are presented in Fig. 1. We resolved a jet-like extension emanating from the AGN core of a distant ($z=4.424$), dust-obscured starburst galaxy, VLA J123642+621331. Together with the previous results, such as morphology, radio spectral index, radio intensity variability, etc., our detections of the compact radio components for the 12 radio sources are the clear evidence of AGN.

4. Radio, IR, and X-ray correlations

We calculated the flux ratio between mid-IR ($24\mu\text{m}$) and radio (1.4 GHz), $q_{24\mu\text{m}}$ [$\equiv \log(S_{24\mu\text{m}}/S_{1.4\text{GHz}})$], and also tested possible correlations between mid-IR, X-ray, and radio luminosities (Fig. 3, Fig. 2). We selected 55 sources detected in all of three catalogs, *Spitzer* MIPS $24\mu\text{m}$ (DR1+, Feb. 2005), *Chandra* 2Ms catalog (Alexander et al. 2003), and VLA 1.4 GHz (Richards et al. 1998). For the comparison of AGN with starbursts (SBs), we classified each source as a SB or an AGN. Since

source classification is still unclear depending on wavelengths, we take only 18 SBs into count, which are classified as SBs in both radio and X-ray domain, and 12 sources, detected by our VLBI observations, represent AGN. We used the SED model by Chary & Elbaz (2001) to calculate the IR luminosities.

The $q_{24\mu\text{m}}$ plot (Fig. 3) shows radio-excess properties (the smaller $q_{24\mu\text{m}}$) of AGN sample ($\langle q_{24\mu\text{m}} \rangle \sim -0.108$). The mean value, $\langle q_{24\mu\text{m}} \rangle$, for SBs is 0.539 ± 0.432 , which is consistent with a previous result of 0.52 ± 0.37 (Beswick et al. 2008). Fig. 2 shows correlations of radio, IR, and X-ray for the SBs. In Fig. 2a and 2b, SBs show a clear correlations of radio/IR and X-ray/IR, while almost AGN are out of the correlations. The radio/X-ray correlation (Fig. 2c) is again well defined for the SBs, and, unlike in the Fig. 2a, b, the AGN seem to also follow this trend. Note, however, that dust-obscured AGN, which have no optical counterpart or very red counterpart (indicated by the shadowed region), are obviously separated from non-obscured ones. For those dust-obscured AGN, since X-ray is more obscured than radio, radio is stronger than X-ray. In this sense, the results of the multi-wavelengths correlations demonstrate the power of deep, high-resolution VLBI imaging in discriminating AGN from distant, dust-enshrouded star-forming galaxies.

References

- Alexander, D. M., et al. 2003, AJ, 126, 539
- Beswick, R. J., et al. 2008, MNRAS, 385, 1143
- Chary, R. & Elbaz, D. 2003, ApJ, 556, 562
- Garrett, M. A., et al. 1999, New A Rev., 43, 519
- Garrett, M. A., et al. 2000, A&A, 361, L41
- Garrett, M. A., et al. 2001, A&A, 366, L5
- Garrett, M. A. 2001, A&A, 384, L19
- Muxlow, T. W. B., et al. 2005, MNRAS, 358, 1159
- Pope, A., et al. 2006, MNRAS, 370, 1185
- Richards, E. A., et al. 1998, AJ, 116, 1039
- Richards, E. A., et al. 1999, ApJ, 526, L73
- Richards, E. A., 2000, ApJ, 533, 611